[Pd$_4$(μ$_3$-SbMe$_3$)$_4$(SbMe$_3$)$_4$]: A Pd(o) Tetrahedron with μ$_3$ Bridging Trimethylantimony Ligands

Sophie L. Benjamin,[†]* Tobias Krämer,[‡]* William Levason,[◊] Mark E. Light,[◊] Stuart A. Macgregor[‡] and Gillian Reid[◊]

[†]School of Science and Technology, Nottingham Trent University, Nottingham NG11 8NS, U.K.; [‡]Institute of Chemical Sciences, Heriot-Watt University, Edinburgh EH14 4AS, U.K.; [◊]School of Chemistry, University of Southampton, Southampton SO17 1BJ, U.K.

Received:

Supporting Information Placeholder

ABSTRACT: The palladium(II) chlorostibine complex [PdCl$_2$(SbMe$_2$Cl)$_2$]$_2$ has a dimeric structure in the solid state, stabilized by hyper-coordination at the Lewis amphoteric Sb centres. Reaction with 8 equivalents of MeLi forms [Pd$_4$(μ$_3$-SbMe$_3$)$_4$(SbMe$_3$)$_4$], whose structure comprises a tetrahedral Pd(0) core with four terminal SbMe$_3$ ligands and four μ$_3$-SbMe$_3$ ligands, one capping each triangular Pd$_3$ face. Density functional theory (DFT) calculations, supported by energy decomposition analysis (EDA) and the natural orbitals for chemical valence (NOCV) scheme, highlight significant donor and acceptor orbital contributions to the bonding between both the terminal and the bridging SbMe$_3$ ligands and the Pd$_4$ core.

Despite their ubiquity in modern coordination chemistry, it was long thought that phosphine ligands and their heavier pnictine congeners (PnR$_3$; Pn = P, As, Sb, Bi) were terminal donors only, while other π-acceptor ligands such as CO are frequently found to bridge more than one metal centre. Werner was the first to challenge this concept, with the isolation of a Rh$_2$ dimer bridged by Sb^{i}Pr$_3$ (Figure 1 i.), its subsequent ligand metathesis giving rise to the first examples of μ$_2$-bridging PR$_3$ and AsR$_3$.[1,2] Despite this breakthrough, very few other systems with bridging pnictines have since been characterized; Balch isolated a few examples of PF$_3$ triply bridging a Pd$_3$ triangle (Figure 1 ii.),[3,4] and Gabbaï recently reported the complexation of a tetradentate P$_3$Pn ligand (Pn = Sb, Bi) with a M$_3$ triangle (M = Cu, Ag) in which the heavy pnictine donor is supported centrally above the M$_3$ face (Figure 1 iii.).[5] Because of the rarity of such species, little is known about the nature of the bonding in these complexes. Based on the limited examples, the bridging mode seems to feature a significant component of acceptance by the ligand, and is best stabilized by late transition metals in low oxidation states, and strongly π-accepting or heavier, more Lewis acidic pnictines.[6]

There has been a surge of recent interest in the 'non-innocent' behavior of coordinated heavy pnictines, which in several cases demonstrate redox reactivity or anion exchange at Pn in preference to the transition metal centre.[7,8] They are also prone to hyper-coordination, forming intra- or intermolecular secondary acceptor interactions with electronegative donor atoms; this behavior is enhanced by electronegative substituents on the pnictine, which increase the Lewis acidity of the Pn centre.[9] We have previously demonstrated that increasing the number of halide substituents in SbBr$_n$Me$_{3-n}$ (n = 0, 1, 2) increases the π-acceptor capacity of the stibine ligand.[10] While triorganopnictines are σ-donor/π-acceptor ligands, halide substituted Sb and Bi centres have been seen to act as σ-acceptors towards electron rich transition metals, giving rise to complexes with highly unusual electronic strutures.[11-14]
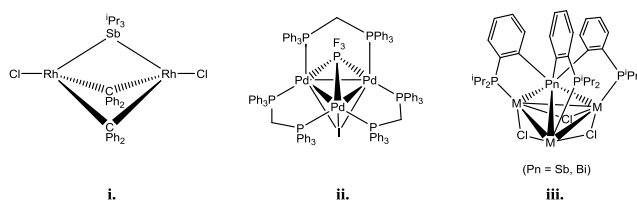

Figure 1. Complexes with bridging pnictine ligands (refs. 1-5)

We report here an unusual dimeric Pd(II) complex of SbMe$_2$Cl which demonstrates significant Lewis acidity of the bound halostibine. The reaction of this complex with MeLi leads to formation of an unexpected Pd(0) cluster featuring both terminal and triply bridging SbMe$_3$ ligands – the first example of an unsupported μ$_3$-organopnictine ligand.

The reaction of [PdCl$_2$(MeCN)$_2$] with two equivalents of SbMe$_2$Cl resulted in the formation of [PdCl$_2$(SbMe$_2$Cl)$_2$] as a red solid in good yield, which appears stable in air for several hours (Scheme 1). The expected singlet was observed in the ^{1}H NMR spectrum, as well as a single broad ^{13}C{^{1}H} NMR resonance. The solid state far IR spectrum shows two bands corresponding to Pd-Cl stretches (C$_{2v}$: A$_1$ + B$_1$). Crystals were grown from the benzene filtrate and analyzed by X-ray crystallography. The solid state structure comprises the centrosymmetric dimeric unit [PdCl$_2$(SbMe$_2$Cl)$_2$]$_2$, consisting of two distorted square planar Pd centres with *cis* chloride and chlorostibine ligands, connected by a fairly short Pd(II)-Pd(II) interaction (2.9143(4) Å) (Figure 2).

Scheme 1. Synthesis of [PdCl₂(SbMe₂Cl)₂]₂ and [Pd₄(μ₃-SbMe₃)₄(SbMe₃)₄]

Scheme 1. Synthesis of $[PdCl_2(SbMe_2Cl)_2]_2$ and $[Pd_4(\mu_3\text{-}SbMe_3)_4(SbMe_3)_4]$
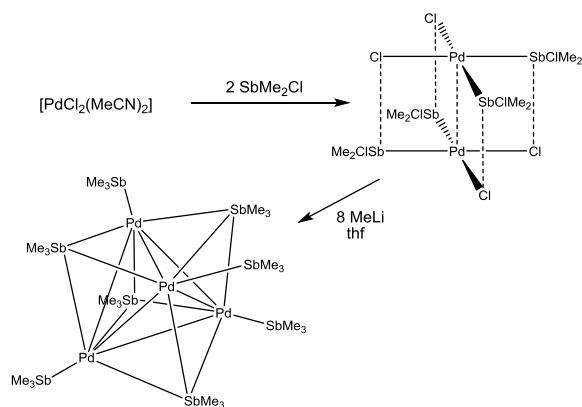
Most examples of Pd(II) dimers feature bidentate bridging ligands supporting the Pd-Pd interaction. One rare counterexample is the diaminosugar complex $[Pd(C_7H_{16}N_2O_2)Cl_2]_2$ (Pd-Pd = 3.284 Å), in which dimerization is supported by H-bonding between amine and Cl ligands.[15] A similar conformation is adopted by $[PdCl_2(SbMe_2Cl)_2]_2$; each chlorostibine ligand eclipses a Cl ligand on the opposite Pd centre when viewed down the Pd-Pd vector (torsion angles: Cl4-Pd1-Pd1a-Sb1a = 3.94(3)° Cl3-Pd1-Pd1a-Sb2a = 5.68(3)°), leading to very short intermolecular Sb-Cl distances (mean 2.96 Å, c.f. mean Sb-Cl covalent = 2.39 Å, ΣVdW = 4.29 Å[16]).
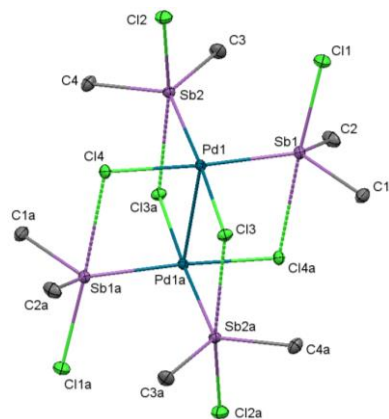

Figure 2. View of the structure of $[PdCl_2(SbMe_2Cl)_2]_2$. Ellipsoids are drawn at 50% probability levels and H atoms are omitted for clarity. Secondary Sb-Cl interactions are indicated by dashed bonds. Symmetry operation a = 2-x,1-y,1-z

The propensity of coordinated Sb or Bi donors to act simultaneously as acceptors, forming intra- or intermolecular 'hypervalent' interactions with electronegative atoms, is a current area of interest,[8,9] and it has been demonstrated that these interactions can strongly direct the solid state structure of a complex.[17] It appears that in $[PdCl_2(SbMe_2Cl)_2]_2$, four such Sb---Cl interactions support the formation of the dimeric species. These interactions form approximately *trans* to the covalently bonded halide substituent on Sb (mean <Cl---Sb-Cl = 169.0°), the Sb-Cl σ* being the most accessible acceptor orbital on Sb. Consistent with this, natural bond orbital (NBO) analysis identifies a notable $3p_{Cl} \rightarrow \sigma^*_{Sb\text{-}Cl}$ interaction (see SI for further details). The geometry at Sb is near trigonal bipyramidal, severely distorted from the expected pseudo-tetrahedral. The structure is reminiscent of that of the Pt(II)-Pt(II) dimer $[PtCl_2\{CH_2(o\text{-}C_6H_4CH_2SbMe_2)\}_2]_2$, which contains weak intermolecular Sb---Cl contacts (mean 3.48 Å);[18] the considerably shorter Sb---Cl distances found in $[PdCl_2(SbMe_2Cl)_2]_2$ can be accounted

for by the increased acceptor power of the halostibine in comparison to the triorganostibine. In each case it is difficult to separate the magnitude of the secondary Sb---Cl interaction from that of the metallophilic interaction between the Group 10 metals.

There are very few previous reports of halostibine complexes with transition metal halides. In view of the recent interest surrounding the 'non-innocent' behavior of coordinated stibines, we investigated the reactivity of $[PdCl_2(SbMe_2Cl)_2]_2$ with reagents which specifically have the potential to target both the Pd and Sb metal centres. Treatment of $[PdCl_2(SbMe_2Cl)_2]_2$ with 8 equivalents of MeLi (equimolar with Cl) in tetrahydrofuran resulted in the formation of an intensely violet solution, from which a dark purple solid was isolated (Scheme 1). The product is stable over several weeks when stored under an N_2 atmosphere, but slowly becomes black/brown in contact with air. It is remarkably soluble in n-hexane, and almost insoluble in chlorinated solvents. Small purple crystals were analysed by X-ray diffraction, giving the solid state structure shown in Figure 3, formulated as $[Pd_4(\mu_3\text{-}SbMe_3)_4(SbMe_3)_4]$.
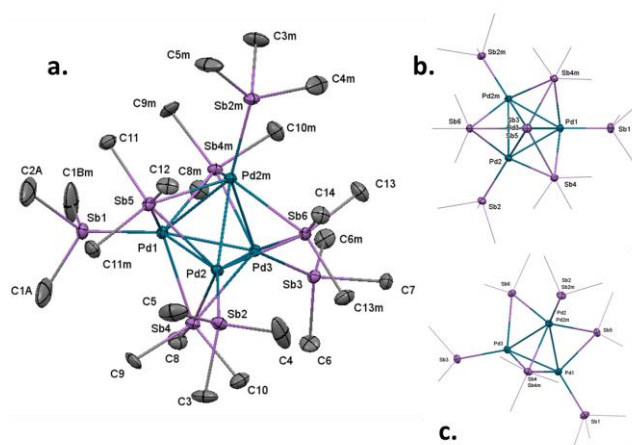

Figure 3. Views of the structure of $[Pd_4(\mu_3\text{-}SbMe_3)_4(SbMe_3)_4]$. Ellipsoids are drawn at 50% probability and H atoms are omitted for clarity. Only one of two symmetry equivalent positions shown for the Me substituents of Sb1. Symmetry operation m = 1-x, +y, +z. **a.** best view; **b.** down a Sb$_{terminal}$-Pd-----Sb$_{bridging}$ vector; **c.** down the a-axis. C atoms are drawn as wireframe in **b.** and **c.**

The structure comprises a central tetrahedron of four Pd(0) atoms, with an average Pd-Pd distance of 2.805 Å. Each Pd is coordinated to one terminal SbMe₃ ligand (mean Pd-Sb = 2.520 Å) and one SbMe₃ ligand caps each face of the tetrahedron, bridging three Pd atoms (mean Pd-Sb = 2.773 Å). A mirror plane bisects the tetrahedron, passing through two Pd atoms, two bridging Sb and two terminal Sb atoms. There is symmetry related disorder of the Me substituents on the terminal Sb1. Each bridging SbMe₃ ligand is almost equidistant from the three Pd atoms it caps – the least symmetrical is Sb5, with a difference of 0.07 Å between Sb5-Pd1 and Sb5-Pd2. The most symmetrical, Sb4, has less than 0.01 Å difference between Sb4-Pd1, Sb4-Pd2 and Sb4-Pd3. The molecule has near C_{3v} symmetry, but attempts to solve the diffraction data in higher symmetry space groups were unsatisfactory; the Cmc2₁ solution is correct. Figure 3b. and c. show alternative views of the structure in which this pseudosymmetry can be clearly discerned.

The ¹H and ¹³C{¹H} NMR spectra of $[Pd_4(\mu_3\text{-}SbMe_3)_4(SbMe_3)_4]$ in d⁶-benzene solution each display two broad resonances of equal intensity, corresponding to two distinct SbMe₃ environments. This is consistent with the conservation of the tetramer in solution, the broadening of the peaks being most likely due to the proximity of the quadrupolar Sb nuclei (^{121}Sb I = 5/2; ^{123}Sb I = 7/2). The identity of the product is supported by elemental analysis.

The triply bridging behavior of a monodentate organopnictine ligand is unprecedented. Of the two systems previously reported which feature μ_3-pnictines, the first involves PF_3, a strong π-acceptor ligand which can be considered as electronically more akin to CO than to PR_3. In $[Pd_3(\mu_3\text{-}PF_3)(\mu\text{-}X)(\mu\text{-}dppm)_3]^+$ (X = Cl, I; dppm = bis(diphenylphosphino)methane) the PF_3 unit bridges an equilateral triangle of Pd(0)/(I) atoms (Figure 1 ii) which bears a significant resemblance to the faces of the Pd(0) tetrahedron discussed here; the Pd-Pd distances are somewhat shorter (2.58-2.60 Å).[3,4] The second (Figure 1, iii), $[M_3(\mu\text{-}Cl)_3(o\text{-}\{^iPr_2P\}C_6H_4)_3Pn]$ (M = Cu, Ag; Pn = Sb, Bi), features a tetradentate ligand in which M-P bonding constrains the heavy pnictogen atom in a bridging position over the centre of the M_3 triangle.[5] NBO calculations demonstrated significant $Pn{\rightarrow}M$ donor interactions as well as weaker $Pn{\leftarrow}M$ acceptor interactions, amounting to a symmetrical four-centre two-electron bridging PnM_3 interaction.

The structure of $[Pd_4(\mu_3\text{-}SbMe_3)_4(SbMe_3)_4]$ is particularly unexpected given that the bridging $SbMe_3$ is unsupported, i.e. not stabilized by polydentate bridging moieties, and that $SbMe_3$ might be expected to be only a moderate π-acceptor. The cluster is held together entirely by μ_3-SbMe$_3$ bridges and Pd-Pd interactions. Comparable $Pd(0)_4$ clusters with terminal phosphines and μ_2-bridging CO or SO_2 ligands have been reported with similar Pd-Pd distances, though they are generally of lower symmetry.[19,20] Recently, the unusual $[\{Pd(CN^tBu)\}_4(GaCp^*)_4]$ cluster was reported, containing a highly symmetric Pd_4Ga_4 core, comparable to the Pd_4Sb_4 core of $[Pd_4(\mu_3\text{-}SbMe_3)_4(SbMe_3)_4]$, with a similar Pd-Pd distance (2.875 Å) and Pd-Ga distances of 2.535 Å.[21]

Density Functional Theory (DFT) was employed to provide insight into the electronic structure of $[Pd_4(\mu_3\text{-}SbMe_3)_4(SbMe_3)_4]$. Full geometry optimization under C_1 symmetry afforded a structure with bond parameters closely matching the crystal structure. However, to facilitate the analysis we have used a C_{3v}-optimized geometry: this lies only 3 kcal mol^{-1} above the C_1 minimum and leaves the approximately tetrahedral geometry essentially unchanged (Table S1 and Figure S1).

The formal cluster electron count of 56 for $[Pd_4(\mu_3\text{-}SbMe_3)_4(SbMe_3)_4]$ is 4 electrons fewer than the predicted valence electron count of 60 for a tetrahedron with localized bonding. Such an ideal count is exemplified in $[Ni_4(CO)_6(P(C_2H_4CN)_3)_4]$ (T_d symmetry),[22] which contains 6 edge-bridging carbonyls and 4 terminal phosphine ligands at the vertices. However, stable electron-deficient clusters are not uncommon for the heavier Group 10 metals,[20,23-26] which often form stable compounds that do not conform to the 18-electron rule, a fact attributed to the increased energy gap between the valence d and p orbitals in these late transition metals. Mingos discussed the electronic structure of the hypothetical $[Pt(PH_3)_2]_4$ clusters, in which terminal PH_3 bonding was assumed, and predicted counts of 56 or 54 electrons depending on the orientation of the ligands.[27]

Both the stability and diamagnetism of the title cluster are borne out in the molecular orbital (MO) diagram (Figure S2). There are 40 electrons that occupy all orbitals of the d manifold, forming a band of MOs centred on the edges and faces of the Pd_4 core. Overlap between symmetry-adapted ($4a_1 + 2e$) ligand group donor orbitals with combinations of metal-based σ-type 5s/5p cluster acceptor orbitals of matching symmetry leads to the formation of bonding MOs, lying energetically below the d block. These orbitals accommodate the 8 donor electron pairs and account for metal-ligand bonding. A considerable gap of ~2 eV separates the LUMO (e_1 symmetry) from the HOMO.

An energy decomposition analysis (EDA)[28,29] was carried out in order to compare the donor-acceptor capabilities of the terminal and face-capping stibine ligands and their interactions with the with the remaining $\{Pd_4(SbMe_3)_7\}$ fragment (Table 1). The terminal $SbMe_3$ ligand exhibits a larger fragment binding energy $-D_e$ (-17.2

kcal mol^{-1}) compared to the face-capping motif (-10.3 kcal mol^{-1}). The face-capping location of the μ_3-SbMe$_3$ ligand over a $\{Pd_3\}$ face results in enhanced interactions relative to the terminal $SbMe_3$ interacting with a single Pd center. Thus μ_3-SbMe$_3$ has a larger ΔE_{steric} (+47.2 kcal mol^{-1} vs. +15.5 kcal/mol) but this is offset by a greater ΔE_{orb} (-65.5 kcal mol^{-1} vs. -37.8 kcal mol^{-1}). The individual contributions to ΔE_{orb} are dominated by the A_1 and E_1 components equating to σ-donation (Sb$\rightarrow$Pd) and π-back donation (Sb$\leftarrow$Pd), respectively; both components are again more significant for the μ_3-SbMe$_3$ ligand. It is striking that for both binding modes the electrostatic term ΔE_{elstat} makes a significantly larger contribution (71-76%) to the total metal-ligand bonding than the orbital term ΔE_{orb} (24-29%). A similar observation has been reported for terminal phosphines,[30] indicating that focussing on orbital interactions alone may be misleading.

Table 1. EDA results of cluster $[Pd_4(\mu_3\text{-}SbMe_3)_4(SbMe_3)_4]$. All energy values in kcal mol^{-1}.

	Terminal	Face-capping
ΔE_{Pauli}	+133.9	+208.9
ΔE_{elstat}[a]	-118.4 (75.8%)	-161.7 (71.2%)
ΔE_{steric}[b]	+15.5	+47.2
ΔE_{orb}[a]	-37.8 (24.2%)	-65.5 (28.8%)
$\Delta E(A_1)$[c]	-21.8 (57.7%)	-32.9 (50.2%)
$\Delta E(A_2)$[c]	-0.3 (0.8%)	-0.8 (1.2%)
$\Delta E(E_1)$[c]	-15.7 (41.5%)	-31.7 (48.4%)
ΔE_{int}	-22.3	-18.3
ΔE_{prep}	+5.1	+8.0
$-D_e$	-17.2	-10.3
$-D_e$ + dispersion	-43.8	-53.6

[a]Values in parentheses give percentage contributions to the total attractive interactions ($\Delta E_{elstat} + \Delta E_{orb}$). [b] $\Delta E_{steric} = \Delta E_{Pauli} + \Delta E_{elstat}$ [c]Values in parentheses give percentage contributions to the total orbital interaction (ΔE_{orb}). [d] $-D_e = \Delta E_{int} + \Delta E_{prep}$

Importantly, the ligand-cluster interactions are further stabilized by dispersion effects, yielding *total* fragment binding energies of -53.6 and -43.8 kcal mol^{-1} for μ_3-SbMe$_3$ and terminal $SbMe_3$, respectively, reversing the order of ligand binding relative to the electronic term alone.

The natural orbitals for chemical valence (NOCV)[31] scheme allows for further insight into the ΔE_{orb} term by highlighting the dominant deformation density channels. Isocontour plots of these channels aid visualization of σ-donation and π-back donation in the cluster (Figure 4). For the terminal case, electron σ-donation from the Sb lone pair (5s) into the vacant Pd acceptor orbital (5s) makes a strong contribution to bonding ($\Delta E^1_{orb} = -14.8$ kcal mol^{-1}). Two components of π-back donation from Pd to Sb can also be clearly identified, and are characterized by energies of $\Delta E^2_{orb} = \Delta E^3_{orb} = -6.0$ kcal mol^{-1}. A similar analysis for the μ_3-SbMe$_3$ fragment reveals an increase in the stabilization energies and associated charge flows for both the σ ($\Delta E^1_{orb} = -24.5$ kcal mol^{-1}) and π channels ($\Delta E^2_{orb} = \Delta E^3_{orb} = -10.5$ kcal mol^{-1}) due to the larger overlap area provided by the Pd_3 face, in line with the EDA analysis.

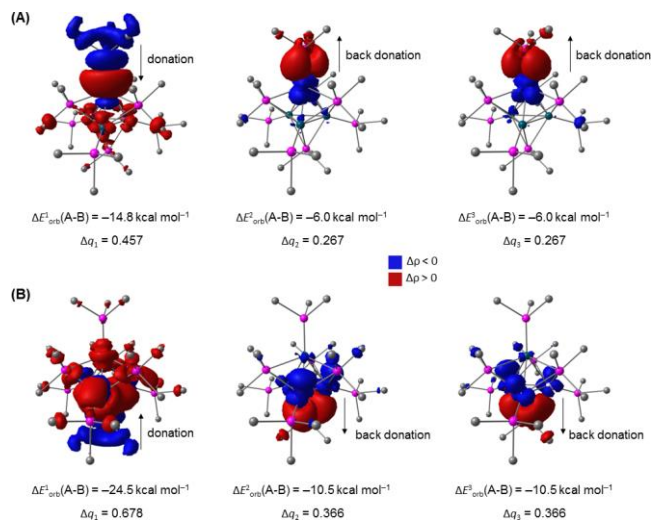**Figure 4.** NOCV contour plots (isovalue 0.0005 a.u.) of key deformation density channels describing the interaction between the cluster fragment $[Pd_4(SbMe_3)_7]$ and a $SbMe_3$ fragment in terminal (panel A) and face-capping (panel B) binding mode. Additionally, corresponding energy eigenvalues ΔE^k_{orb} and charges Δq_k are shown. Electron flow is shown from blue to red.

To summarize, a rare example of a halostibine complex with a transition metal halide has been synthesized and characterized as a dimer in the solid state, supported by secondary Sb---Cl interactions. This complex demonstrates unexpected reactivity with MeLi, resulting in isolation of a highly unusual Pd(0)$_4$ cluster with μ_3-SbMe$_3$ ligands, the first example of triple bridging by a monodentate organopnictine. Computational modelling of the cluster reveals that both bridging and terminal SbMe$_3$ ligands can be efficient acceptors in metal-to-ligand π-back donation, helping to stabilize the electron rich {Pd$_4$} core. Investigation of potential phosphine and arsine analogues is underway in our group. The effect of this new pnictine bonding mode on the electronic environment of the transition metal could have considerable impacts in organometallic chemistry, including in the design of new homogeneous catalysts.

Associated content

Supporting information: further computational analysis of $[Pd_4(\mu_2\text{-}SbMe_3)_6(SbMe_3)_4]$, $[PdCl_2(SbMe_2Cl)_2]_2$ and the hypothetical $[Pd_4(\mu_3\text{-}SbMe_3)(\mu_2\text{-}SbMe_3)_3(SbMe_3)_4]$, computational methods, experimental details, crystallographic information. This material is available free of charge via the Internet at http://pubs.acs.org.

Acknowledgements

References

1. Schwab, P.; Mahr, N.; Wolf, J.; Werner, H. *Angew. Chem. Int. Ed.* **1994**, *33*, 97-99.
2. Werner, H. *Angew. Chem. Int. Ed.* **2004**, *43*, 938-954.
3. Balch, A. L.; Davis, B. J.; Olmstead, M. M. *Inorg. Chem.* **1993**, *32*, 3937-3942.
4. Balch, A. L.; Davis, B. J.; Olmstead, M. M. *J. Am. Chem. Soc.* **1990**, *112*, 8592-8593.
5. Ke, I.; Gabbaï, F. P. *Aust. J. Chem.* **2013**, *66*, 1281-1287.
6. Schinzel, S.; Muller, R.; Riedel, S.; Werner, H.; Kaupp, M. *Chem. Eur. J.* **2011**, *17*, 7228-7235.
7. Ke, I.; Jones, J. S.; Gabbaï, F. P. *Angew. Chem. Int. Ed.* **2014**, *53*, 2633-2637.
8. Wade, C. R.; Ke, I.; Gabbaï, F. P. *Angew. Chem. Int. Ed.* **2012**, *51*, 478-481.
9. Benjamin, S. L.; Reid, G. *Coord. Chem. Rev.* **2015**, *297–298*, 168-180.
10. Benjamin, S. L.; Levason, W.; Reid, G.; Warr, R. P. *Organometallics* **2012**, *31*, 1025-1034.
11. Braunschweig, H.; Dewhurst, R. D.; Hupp, F.; Wolf, J. *Chem. Eur. J.* **2015**, *21*, 1860-1862.
12. Tschersich, C.; Limberg, C.; Roggan, S.; Herwig, C.; Ernsting, N.; Kovalenko, S.; Mebs, S. *Angew. Chem. Int. Ed.* **2012**, *51*, 4989-4992.
13. Lin, T.; Ke, I.; Gabbaï, F. P. *Angew. Chem. Int. Ed.* **2012**, *51*, 4985-4988.
14. Ke, I.; Gabbaï, F. P. *Inorg. Chem.* **2013**, *52*, 7145-7151.
15. Samochocka, K.; Fokt, I.; Anulewicz-Ostrowska, R.; Przewloka, T.; Mazurek, A. P.; Fuks, L.; Lewandowski, W.; Kozerski, L.; Bocian, W.; Bednarek, E.; Lewandowska, H.; Sitkowski, J.; Priebe, W. *Dalton Trans.* **2003**, 2177-2183.
16. Alvarez, S. *Dalton Trans.* **2013**, *42*, 8617-8636.
17. Benjamin, S. L.; Levason, W.; Light, M. E.; Reid, G.; Rogers, S. M. *Organometallics* **2014**, *33*, 2693-2695.
18. Brown, M. D.; Levason, W.; Reid, G.; Webster, M. *Dalton Trans.* **2006**, 5648-5654.
19. Burrows, A. D.; Mingos, D. M.; Menzer, S.; Vilar, R.; Williams, D. J. *J. Chem. Soc. Dalton Trans.* **1995**, 2107-2108.
20. Dubrawski, J.; Kriege-Simondsen, J.; Feltham, R. D. *J. Am. Chem. Soc.* **1980**, *102*, 2089-2091.
21. Molon, M.; Dilchert, K.; Gemel, C.; Seidel, R.; Schaumann, J.; Fischer, R. A. *Inorg. Chem.* **2013**, *52*, 14275-14283.
22. Bennett, M. J.; Cotton, F. A.; Winquist, B. H.; *J. Am. Chem. Soc.* **1967**, *89*, 5366-5372.
23. Mednikov, E. G.; Eremenko, N. K.; Gubin, S. P.; Slovokhotov, Y. L.; Struchkov, Y. T. *J. Organomet. Chem.* **1982**, *239*, 401-416.
24. Feltham, R. D.; Elbaze, G.; Ortega, R.; Eck, C.; Dubrawski, J. *Inorg. Chem.* **1985**, *24*, 1503-1510.
25. Burrows, A. D.; Machell, J. C.; Mingos, D. M. P. *J. Chem. Soc. Dalton Trans.* **1992**, 1991-1995.
26. Frost, P. W.; Howard, J. A. K.; Spencer, J. L.; Turner, D. G. *J. Chem. Soc. Chem. Commun..* **1981**, 1104-1106.
27. Evans, D.; Mingos, D. M. P *J. Organomet. Chem.* **1982**, *240*, 312-327.
28. Morokuma, K. *J. Chem. Phys.* **1971**, *55*, 1236-1244.
29. Ziegler, T.; Rauk, A. *Theor. Chim. Acta.* **1977**, *46*, 1-10.
30. Frenking, G.; Wichmann, K.; Fröhlich, N.; Loschen, C.; Lein, M.; Frunzke, J.; Rayón, V. M. *Coord. Chem. Rev.* **2003**, *238*, 55-82.
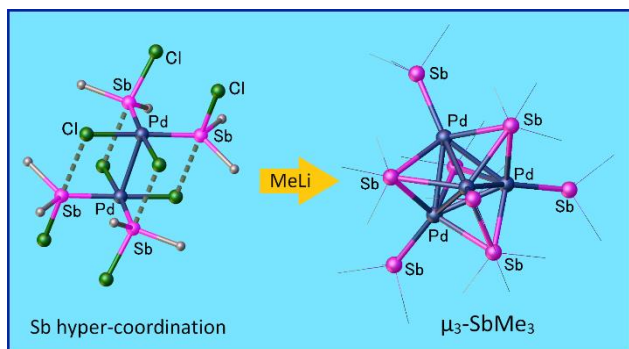31. Mitoraj. M. P.; Michalak, A.; Ziegler, T. *J. Chem. Theor. Comput.* **2009**, *5*, 962-97.

Table of Contents Graphic